IEEE Photonics Journal
An IEEE Photonics Society Publication

Open Access

Calibration Method for Division-of-Focal-Plane Polarimeters Using Nonuniform Light

Volume 13, Number 1, February 2021

Zhichao Ding
Chunsheng Sun
Hongwei Han
Liheng Ma
Yonggang Zhao

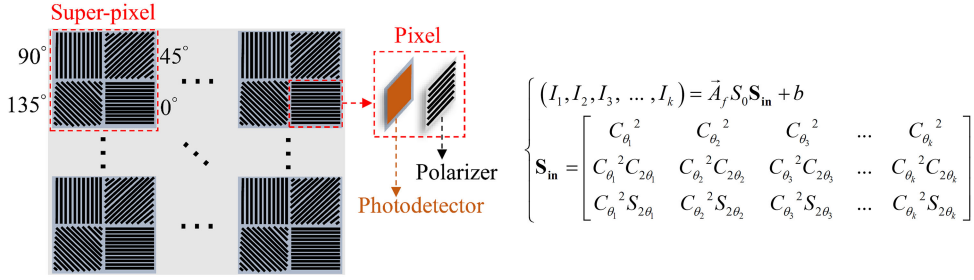

$$\vec{A}_{fc} = \mathbf{S}_{in}^{+} \left(I_1 - b_c, I_2 - b_c, I_3 - b_c, \ldots, I_k - b_c \right)$$

DOI: 10.1109/JPHOT.2020.3048007

Calibration Method for Division-of-Focal-Plane Polarimeters Using Nonuniform Light

Zhichao Ding, Chunsheng Sun, Hongwei Han, Liheng Ma, and Yonggang Zhao

College of Ordnance Engineering, Naval University of Engineering, Wuhan 430033, China

DOI:10.1109/JPHOT.2020.3048007

Manuscript received September 19, 2020; revised December 3, 2020; accepted December 24, 2020. Date of publication December 29, 2020; date of current version January 14, 2021. Corresponding author: Chunsheng Sun (e-mail: scs96581@163.com).

Abstract: A method to calibrate the errors of polarization information measured by division-of-focal-plane polarimeters is demonstrated. The principle of this method is explained, and its feasibility is verified by theoretical simulation and experiment. The simulation and experimental results show that this method can obviously improve the measuring precision of polarization information, and compared with other approaches, the proposed method just uses normal light sources, but can achieve comparable performance.

Index Terms: DoFP polarimeters, polarization information, image calibration.

1. Introduction

Intensity, frequency, phase and polarization are four crucial parameters of the light. A normal camera can record the intensity and frequency of the light which are characterized by the brightness and color of image pixels, respectively, but cannot acquire the information of polarization. However, the application value of polarization information has been being discovered in various of fields, ranging from image contrast enhancement, like remote sensing and polarization-based dehazing [1]–[5], to bionics and biomedical imaging [6]–[9].

In order to achieve the polarization information, several kinds of polarization imaging sensors are designed, which can be summarized as four main types: division-of-aperture polarimeter [10], division-of-amplitude polarimeter [11], division-of-time polarimeter [12], and division-of-focal-plane (DoFP) polarimeter [13]–[16]. Among these polarization imaging sensors, DoFP polarimeters are always recommended for their compact structure and ability of real-time polarization information detection.

The basic unit of a DoFP polarimeter is the pixel which is composed by a linear polarizer and a photodetector (CCD or CMOS) as shown in Fig. 1. When the incident light reaches a pixel, it is firstly filtered by the linear polarizer, and then the transmitted part is detected by the photodetector of this pixel. Every four adjacent pixels with their linear polarizers orienting 0°, 45°, 90° and 135°, respectively, are grounded into a 2 by 2 super-pixel, and these super-pixels side by side combine the DoFP polarimeter as shown in Fig. 1. Since a super-pixel can obtain the intensity components of light polarizing along four different orientations, the polarization information characterized by

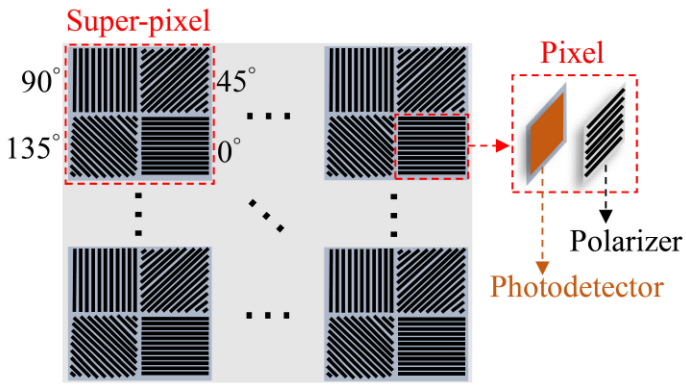

Fig. 1. Schematic diagram of the DoFP polarimeter.

degree of polarization (DoP) and angle of polarization (AoP) can be derived for the light incident on the super-pixel [17].

Ideally, the DoP and AoP measured by the DoFP polarimeter can accurately reflect the polarization information of the incident light. However, due to the manufacturing defects and system noise, there are some differences between the measured and actual results. For this reason, the DoFP polarimeter needed to be calibrated for minimizing the measuring errors of polarization information. Several prior attempts to calibrate DoFP polarimeters were reported. For instances, Power and Gruev evaluated a scalar and matrix calibration derived from a mathematical model of the polarimeter behavior [15], Zhang *et al.* uses the average analysis matrix to replace the ideal analysis matrix adopted in Ref [15] to calibrate DoFP polarimeters [19], and Fei *et al.* realized the calibration by fitting the relationship of input and output light intensities under different DoP and AoP of the incident light [20].

In the above common calibrating approaches, a uniform light source is necessary to generate uniform and unpolarized incident light. However, the uniform light source is costly and not available in the normal labs. In addition, the usage of the uniform light source adds the complexity of the calibrating setup. Given all this, in this paper, we demonstrate the feasibility to calibrate DoFP polarimeters using ordinary light source, and a calibration method is proposed to realize it.

2. Theoretical Model

Assume that the light incident on anyone of super-pixels is uniform. For the light incident on a super-pixel, it is represented by the linear Stokes vector $\vec{S}_i = [S_{i0}, S_{i0}P_i\cos(2\theta_i), S_{i0}P_i\sin(2\theta_i), 0]^{\mathrm{T}}$, where S_{i0}, P_i and θ_i are the intensity, DoP and AoP of the incident light, respectively. Considering one pixel of this super-pixel firstly, the light transmitted by the linear polarizer of this pixel is represented by the Stokes vector $\vec{S}_o = [S_{o0}, S_{o0}P_o\cos(2\theta_o), S_{o0}P_o\sin(2\theta_o), 0]^{\mathrm{T}}$, where S_{o0}, P_o and θ_o are the intensity, DoP and AoP of the transmitted light, respectively. The relationship between $\vec{S}_i$ and $\vec{S}_o$ is given by

$$\vec{S}_o = \mathbf{M_{lp}}\vec{S}_i, \tag{1}$$

where $\mathbf{M_{lp}}$ is the Mueller matrix for the linear polarizer of the pixel. For the linear polarizer with the orientation of θ, $\mathbf{M_{lp}}$ can be obtained by the following equation:

$$\mathbf{M_{lp}} = \frac{1}{2}\begin{bmatrix} q+r & (q-r)C_{2\theta} & (q-r)S_{2\theta} & 0 \\ (q-r)C_{2\theta} & (q+r)C_{2\theta}^2 + 2\sqrt{qr}S_{2\theta}^2 & \left(q+r-2\sqrt{qr}\right)S_{2\theta}C_{2\theta} & 0 \\ (q-r)S_{2\theta} & \left(q+r-2\sqrt{qr}\right)S_{2\theta}C_{2\theta} & (q+r)S_{2\theta}^2 + 2\sqrt{qr}C_{2\theta}^2 & 0 \\ 0 & 0 & 0 & 4\sqrt{qr} \end{bmatrix}. \tag{2}$$

Here, q and r are, respectively, the major and minor light transmittances of the linear polarizer, $C_{2\theta} = \cos(2\theta)$, and $S_{2\theta} = \sin(2\theta)$.

The light transmitted by the linear polarizer is detected by the photodetector of the pixel, and the signal I outputted by the photodetector satisfies

$$I = gS_{00} + b. \tag{3}$$

Here, g and b are the gain and dark offset of the photodetector, respectively. Defining the analysis vector $\vec{A}_f = \frac{g}{2}[q + r, (q - r)C_{2\theta}, (q - r)S_{2\theta}]$, and simplifying $\vec{S}_i$ as $[S_{i0}, S_{i0}P_i\cos(2\theta_i), S_{i0}P_i\sin(2\theta_i)]^{\mathrm{T}}$, (3) can be rewritten as

$$I = \vec{A}_f\vec{S}_i + b. \tag{4}$$

For the super-pixel, the output signals can be stacked a column vector $\vec{I}_{sp} = (I_0, I_{45}, I_{90}, I_{135})^{\mathrm{T}}$

$$\vec{I}_{sp} = \begin{pmatrix} I_0 \\ I_{45} \\ I_{90} \\ I_{135} \end{pmatrix} = \begin{pmatrix} \vec{A}_{f,0} \\ \vec{A}_{f,45} \\ \vec{A}_{f,90} \\ \vec{A}_{f,135} \end{pmatrix} \vec{S}_i + \begin{pmatrix} b_0 \\ b_{45} \\ b_{90} \\ b_{135} \end{pmatrix} = \mathbf{A}\vec{S}_i + \vec{b}_{sp}. \tag{5}$$

Here, $\mathbf{A}$ is the analysis matrix for the super-pixel, $\vec{A}_{f,0}$, $\vec{A}_{f,45}$, $\vec{A}_{f,90}$ and $\vec{A}_{f,135}$ are the analysis vectors for the pixels with the linear polarizers orienting 0°, 45°, 90° and 135°, respectively, and b_0, b_{45}, b_{90} and b_{135} are corresponding dark offsets. When $\vec{I}_{sp}$ is obtained, the polarization information detected by the super-pixel can be derived

$$\begin{cases} P_t = \sqrt{(I_0 - I_{90})^2 + (I_{45} - I_{135})^2} / (I_0 + I_{90}) \\ \theta_t = \frac{1}{2}\ \mathrm{atan}\ [(I_{45} - I_{135}) / (I_0 - I_{90})] \end{cases}. \tag{6}$$

Here, P_t and θ_t are the detected DoP and AoP of the light incident on the super-pixel, respectively.

As for the ideal DoFP polarimeter, $r = 0$, $b = 0$, $g = g_0$, $q = q_0$ and $\theta = \theta_0$, where g_0 and q_0 are invariant for all the pixels of a super-pixel, and the value of θ_0 is exactly 0°, 45°, 90° or 135°. Under this situation, the analysis matrix $\mathbf{A}$ is proportional to the ideal analysis matrix $\mathbf{A}_i$, $\mathbf{A} = g_0q_0\mathbf{A}_i$, where

$$\mathbf{A}_i = \begin{bmatrix} 1 & 1 & 0 \\ 1 & 0 & 1 \\ 1 & -1 & 0 \\ 1 & 0 & -1 \end{bmatrix}. \tag{7}$$

According to (5)–(7), the detected polarization information by a super-pixel is identical to that of the light incident on the super-pixel.

However, for the actual DoFP polarimeter, $r \neq 0$, $b \neq 0$, g and q are variant for all the pixels of a super-pixel, and the value of θ deviates from 0°, 45°, 90° or 135°, causing the measuring error of polarization information. Notably, if the light incident on a super-pixel is nonuniform, this super-pixel cannot achieve the actual polarization information of light even for the ideal DoFP polarimeter.

3. Calibration Method

The calibration method proposed by this paper is based on the assumption that the light incident on anyone of super-pixels can be regarded as uniform for ordinary light source, since the size of the super-pixel is just several micrometers for common DoFP polarimeters.

According to the above theoretical analysis, in order to minimize the measuring error of polarization information, $\vec{b}_{sp}$ should be compensated, and the analysis matrix $\mathbf{A}$ should be derived. When the compensating value $\vec{b}_c$ of $\vec{b}_{sp}$ and the derived value $\mathbf{A_c}$ of $\mathbf{A}$ are obtained, the calibrating result $\vec{I}_c$ of $\vec{I}_{sp}$ is given by

$$\vec{I}_c = g_0q_0\mathbf{A}_i\mathbf{A_c}^{+}\left(\vec{I}_{sp} - \vec{b}_c\right). \tag{8}$$

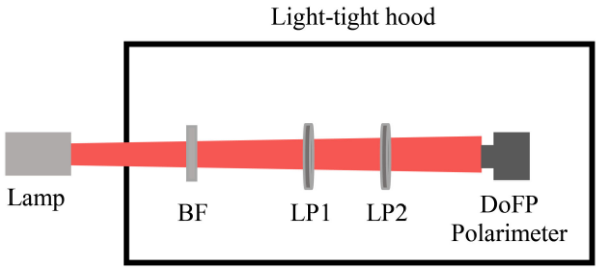

Fig. 2. Experimental setup. BF: bandpass filter, LP: linear polarizer.

Here, $\mathbf{A_c}^+$ is the pseudo-inverse of $\mathbf{A_c}$. As can be seen from (6), when using $\vec{I_c}$ to derive P_t and θ_t, P_t and θ_t are unrelated to $g_0 q_0$, so $\vec{I_c}$ can be simply given by

$$\vec{I_c} = \mathbf{A}_i \mathbf{A_c}^+ \left(\vec{I_{sp}} - \vec{b_c}\right). \tag{9}$$

Since $\vec{b_c} \approx \vec{b_{sp}}$ and $\mathbf{A_c} \approx \mathbf{A}$,

$$\vec{I_c} \approx \mathbf{A}_i \mathbf{A}^+ \left(\mathbf{A}\vec{S_i} + \vec{b_{sp}} - \vec{b_c}\right) \approx \mathbf{A}_i \vec{S_i}, \tag{10}$$

where $\mathbf{A}^+$ is the pseudo-inverse of $\mathbf{A}$. According to (6) and (10), the measuring error of polarization information can decrease dramatically if $\vec{b_c}$ and $\mathbf{A_c}$ are obtained and approximate to $\vec{b_{sp}}$ and $\mathbf{A}$, respectively.

For compensating $\vec{b_{sp}}$, we can record the output signals of the DoFP polarimeter when no light inputs, and the compensating value $\vec{b_c}$ of $\vec{b_{sp}}$ is

$$\vec{b_c} = \vec{I_{sp}}\big|_{S_{i0}=0}. \tag{11}$$

For deriving the analysis matrix using ordinary light source, the following experimental scheme is designed, and the experimental setup is shown in Fig. 2. Partially polarized light is generated by a tungsten halogen lamp or other light sources. It is firstly filtered by a bandpass filter (Thorlabs FB680-10), and then converted to the polarized light after passing through a linear polarizer (LP1, Thorlabs LPVISC100-MP2). Another linear polarizer (LP2, Thorlabs LPVISC100-MP2) is used to adjust the intensity and AoP of the light incident on a DoFP polarimeter. The bandpass filter, LP1, LP2 and the DoFP polarimeter are placed inside a light-tight hood to avoid the disturbance of stray light.

The relative orientations between LP1, LP2 and the linear polarizers of the DoFP polarimeter are determined firstly. Place an optical power meter behind LP2, rotate LP2, and observe the light power. When the light power is minimum, the orientations of LP1 and LP2 are orthogonal. Remove the optical power meter, rotate LP1 and LP2, maintain that the orientations of LP1 and LP2 are collinear, and calculate the mean value of the outputs for all the pixels with their linear polarizers orienting 90°. When the mean value is minimum, record the orientations of LP1 and LP2 and set them as 0°.

The orientation of LP1 is kept at 0°. By rotating LP2 and recording the output of DoFP polarimeter, we can obtain different outputs under various of inputs. For anyone of pixel,

$$\begin{cases} (I_1, I_2, I_3, \ldots, I_k) = \vec{A}_f S_0 \mathbf{S_{in}} + b \\ \mathbf{S_{in}} = \begin{bmatrix} {C_{\theta_1}}^2 & {C_{\theta_2}}^2 & {C_{\theta_3}}^2 & \ldots & {C_{\theta_k}}^2 \\ {C_{\theta_1}}^2 C_{2\theta_1} & {C_{\theta_2}}^2 C_{2\theta_2} & {C_{\theta_3}}^2 C_{2\theta_3} & \ldots & {C_{\theta_k}}^2 C_{2\theta_k} \\ {C_{\theta_1}}^2 S_{2\theta_1} & {C_{\theta_2}}^2 S_{2\theta_2} & {C_{\theta_3}}^2 S_{2\theta_3} & \ldots & {C_{\theta_k}}^2 S_{2\theta_k} \end{bmatrix}. \end{cases} \tag{12}$$

Here, $I_k (k = 1, 2, 3 \ldots)$ is the output of this pixel when the orientation of LP2 is adjusted to $\theta_k (k = 1, 2, 3 \ldots)$, S_0 is the intensity of light incident on the super-pixel containing this pixel when

the orientation of LP2 is equal to 0°, $\mathbf{S_{in}}$ is the input matrix which is the same for all the pixels, ${C_{\theta_k}}^2 = \cos^2(\theta_k)$, $C_{2\theta_k} = \cos(2\theta_k)$, and $S_{2\theta_k} = \sin(2\theta_k)$.

The compensating value b_c of b is given by (11), so we can obtain

$$\vec{A_f} S_0 \mathbf{S_{in}} \approx (I_1 - b_c, I_2 - b_c, I_3 - b_c, \ldots, I_k - b_c)\,. \tag{13}$$

As $(S_0\mathbf{S_{in}})^+ = \frac{1}{S_0}{\mathbf{S_{in}}}^+$, (13) can be calculated as follow

$$\vec{A_f} \approx \frac{1}{S_0}{\mathbf{S_{in}}}^+ (I_1 - b_c, I_2 - b_c, I_3 - b_c, \ldots, I_k - b_c)\,, \tag{14}$$

where $(S_0\mathbf{S_{in}})^+$ and ${\mathbf{S_{in}}}^+$ represent the pseudo-inverse of $S_0\mathbf{S_{in}}$ and $\mathbf{S_{in}}$, respectively.

As can be derived from (6), P_t and θ_t are unrelated to $\frac{1}{S_0}$. Therefore, the derived value $\vec{A}_{fc}$ of $\vec{A}_f$ can be simply given by

$$\vec{A}_{fc} = {\mathbf{S_{in}}}^+ (I_1 - b_c, I_2 - b_c, I_3 - b_c, \ldots, I_k - b_c)\,. \tag{15}$$

Based on (15), we can obtain $\mathbf{A_c}$ for all the super-pixel.

4. Simulation and Experiment

In order to verify the feasibility of the proposed method, simulation and experiment have been done. We first discuss the simulation. The DoFP polarizer with the resolution of $m \times n$ is emulated using following settings. For any linear polarizer of the DoFP polarizer, it is generated according to

$$\begin{cases} q = 0.8 + 0.1 \times \text{rand}(1),\ r = 0.1 \times \text{rand}(1) \\ \theta_0 = -\frac{\pi}{60} + \frac{\pi}{30} \times \text{rand}(1) \\ \theta_{45} = \frac{\pi}{4} - \frac{\pi}{60} + \frac{\pi}{30} \times \text{rand}(1) \\ \theta_{90} = \frac{\pi}{2} - \frac{\pi}{60} + \frac{\pi}{30} \times \text{rand}(1) \\ \theta_{135} = \frac{3\pi}{4} - \frac{\pi}{60} + \frac{\pi}{30} \times \text{rand}(1). \end{cases} \tag{16}$$

Here, rand(1) represents generating a random number between 0 and 1, θ_0, θ_{45}, θ_{90} and θ_{135} are the set orientations when the linear polarizer orients 0°, 45°, 90° and 135° under ideal situation, respectively. For the photodetectors of the DoFP polarizer, they are generated according to

$$\begin{cases} \mathbf{g} = 10 \times \text{rand}(m, n) \\ \mathbf{b} = \left|\text{wgn}(m, n, -30)\right| \end{cases}. \tag{17}$$

Here, rand(m, n) represents generating a $m \times n$ matrix with its numbers between 0 and 1, wgn(m, n, –30) represents generating a $m \times n$ matrix of white Gaussian noise with its power of –30 dB, $\mathbf{g}$ and $\mathbf{b}$ are the matrixes for the gains and dark offsets of the photodetectors, respectively.

For simulating the light generated by a normal light source, the light incident on anyone of super-pixels is set to be uniform, and the light incident on the $\frac{m}{2} \times \frac{n}{2}$ super-pixels of the DoFP is set to that

$$\begin{cases} \mathbf{S_{i0}} = \text{rand}(\frac{m}{2}, \frac{n}{2}) \\ \mathbf{P_i} = \text{rand}(\frac{m}{2}, \frac{n}{2}) \\ \boldsymbol{\theta_i} = -\frac{\pi}{2} + \pi \times \text{rand}(\frac{m}{2}, \frac{n}{2}) \end{cases}, \tag{18}$$

where $\mathbf{S_{i0}}$, $\mathbf{P_i}$ and $\boldsymbol{\theta_i}$ are the $\frac{m}{2} \times \frac{n}{2}$ matrixes respectively for the intensities, DoP and AoP of the light incident on the $\frac{m}{2} \times \frac{n}{2}$ super-pixels.

Using the proposed method and the set incident light, the emulating DoFP polarizer is calibrated. Figure 3 shows a simulation result when $m = 306$ and $n = 256$. In Fig. 3, $\mathbf{P_{it}}$ and $\mathbf{P_{ic}}$ are the detected and calibrated DoP for the light incident on the $\frac{m}{2} \times \frac{n}{2}$ super-pixels, respectively, $\boldsymbol{\theta_{it}}$ and $\boldsymbol{\theta_{ic}}$ are the detected and calibrated AoP for the light incident on the $\frac{m}{2} \times \frac{n}{2}$ super-pixels, respectively. As can be seen in Fig. 3, before calibration, the detected DoP and AoP have evident differences compared with the input DoP and AoP, and the rms of $\mathbf{P_i} - \mathbf{P_{it}}$ and $\boldsymbol{\theta_i} - \boldsymbol{\theta_{it}}$ are as large as 0.0752 and 29.0606 deg, respectively. However, after calibration, there are almost no differences between

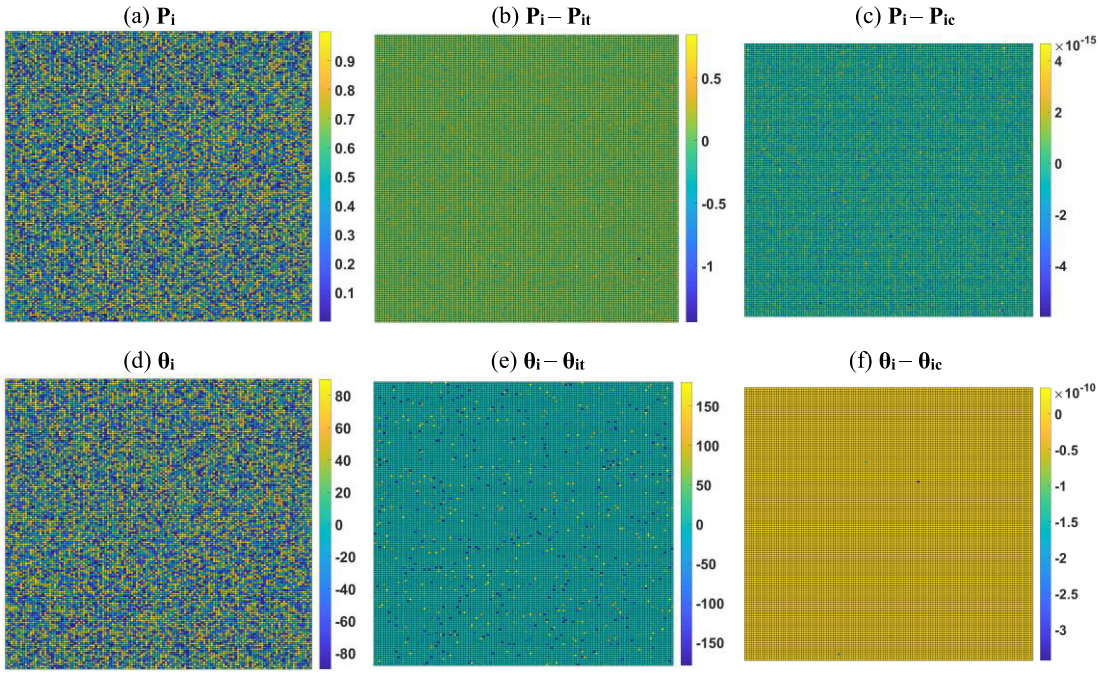

Fig. 3. Simulation results of the proposed method.

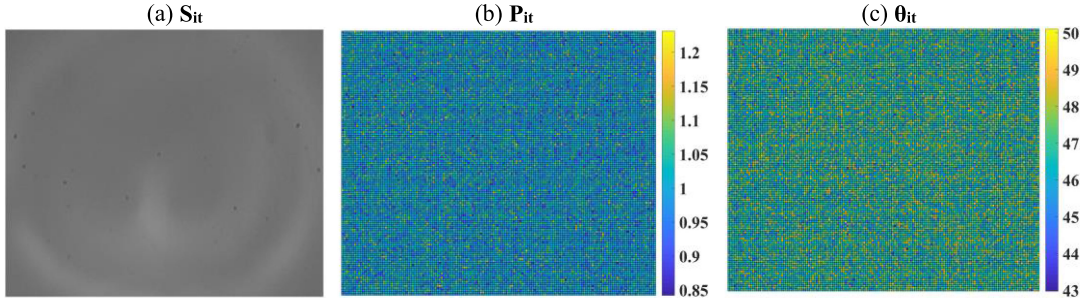

Fig. 4. Experiment results for the DoP and AoP detected by the DoFP.

the input and calibrated DoP and AoP, and the rms of $\mathbf{P_i} - \mathbf{P_{it}}$ and $\boldsymbol{\theta_i} - \boldsymbol{\theta_{it}}$ are only 7.0165 $\times$ 10^{-16} and 2.9907 $\times$ 10^{-12} deg, respectively. The calibration method is also verified under many other simulation conditions, and the results are similar to that shown in Fig. 3, demonstrating the excellent performance of the proposed calibration method.

Then, we discuss the experiment results. The experimental setup is shown in Fig. 2, and a DoFP polarimeter with the model of FLIR BFS-U3-51S5P is selected. When the orientation θ_k of LP2 is approximate to 90°, the intensity of the light incident on the DoFP polarimeter is small, causing a low signal-to-noise ratio and thus affecting the calibration. With that in mind, θ_k is adjusted from 0° to 60° and from 120° to 180° with the step of 2°. An experiment result for the intensity $\mathbf{S_{it}}$, DoP $\mathbf{P_{it}}$ and AoP $\boldsymbol{\theta_{it}}$ detected by the DoFP is shown in Fig. 4. In order to clearly depict the results of $\mathbf{P_{it}}$ and $\boldsymbol{\theta_{it}}$, the false-color images of Fig. 4(b) and Fig. 4(c) are the down-sampling results.

As shown in Fig. 4(a), though the intensity of the incident light is non-uniform in the whole photosensitive region of the DoFP polarimeter, the rms values for the vast majority of 2 $\times$ 2 regions in Fig. 4(a) are smaller than 0.015, demonstrating that the degree of uniformity for a small region

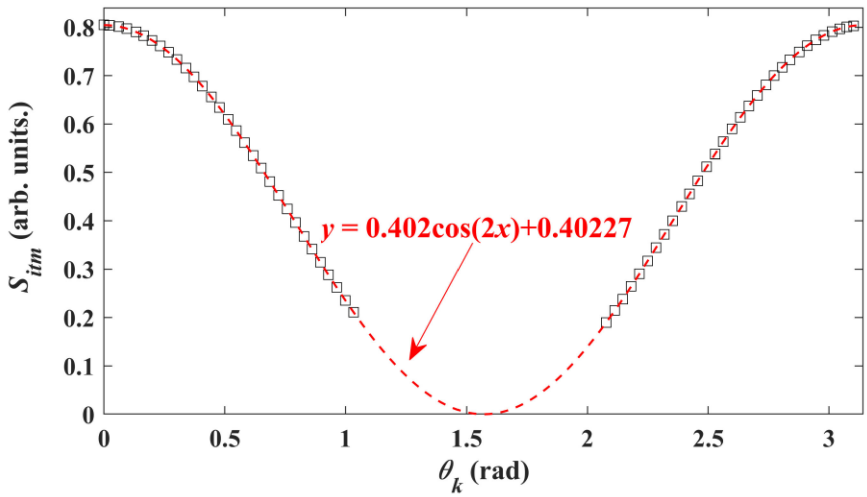

Fig. 5. Fitting result of S_{itm}.

containing at least a super-pixel is rather high, and satisfying the assumption for the proposed calibration method. In addition, the measuring error of polarization information can be obviously seen from Fig. 4(b) and 4(c). So, the calibration is necessary for obtaining a higher measuring precision.

According to the theoretical analysis of last section, in order to derive $\mathbf{A_c}$, the key is to obtain $\mathbf{S_{in}}$ which is determined by θ_k. Though θ_k is adjusted by rotating LP2 which is installed on a high-precision rotation mount (Thorlabs PRM1), there is a remarkable error for θ_k if just observing the scale of PRM1. So, the fitting method is adopted to determine θ_k, and the specific techniques are as below. Firstly, the mean value S_{itm} of $\mathbf{S_{it}}$ is recorded when θ_k is adjusted from 0° to 180°. Then the function

$$y = C_1 \cos(2x + C_2) + C_1 + b_m \tag{19}$$

is used to fitting S_{itm}. Here, C_1 and C_2 are two parameters, and b_m is set as the value of S_{itm} when the light is blocked to reach the DoFP polarimeter. The fitting result is shown in Fig. 5. Based on the fitting result, θ_k is determined, and $\mathbf{A_c}$ is derived based on (12) and (15).

In order to verify the effect of calibration, the BF in the experimental setup is removed, θ_k is adjusted to different orientations, and the DoFP polarimeter records the polarization image under the white (unfiltered) incident light. Using the derived $\mathbf{A_c}$, the calibrating polarization image I_c is obtained based on (9). Figs. 6 and 7 show the measuring rms errors before and after calibration under different S_{itm}. When S_{itm} is relatively large, the detecting system possesses higher signal-to-noise ratio, and thus the measuring error is relatively small. As a result, with the increase of S_{itm}, the measuring errors of DoP and AoP decrease first and then tend to be stable as shown in Figs. 6 and 7, and they are rather low under large S_{itm} no matter before or after calibration. While S_{itm} is not large enough, as can be seen from Figs. 6 and 7, the proposed calibration method can improve the measuring precision of DoP to a great extent (∼40%). Though the measuring error slightly (∼10%) grows after calibration which is mainly due to that the light incident on anyone of super-pixels is not absolutely uniform, it maintains a low level which is smaller than 1 deg. The experimental results demonstrate that the proposed calibration method can lower the measuring error of polarization information significantly.

Comparing the theoretical and experimental results, we can find that under experimental condition, the proposed method cannot reach the perfect performance achieved by theoretical simulation. There are some reasons for that, like the imperfect experimental setups, quantization error, and pixel-to-pixel crosstalk. Nevertheless, compared with other approaches which can control

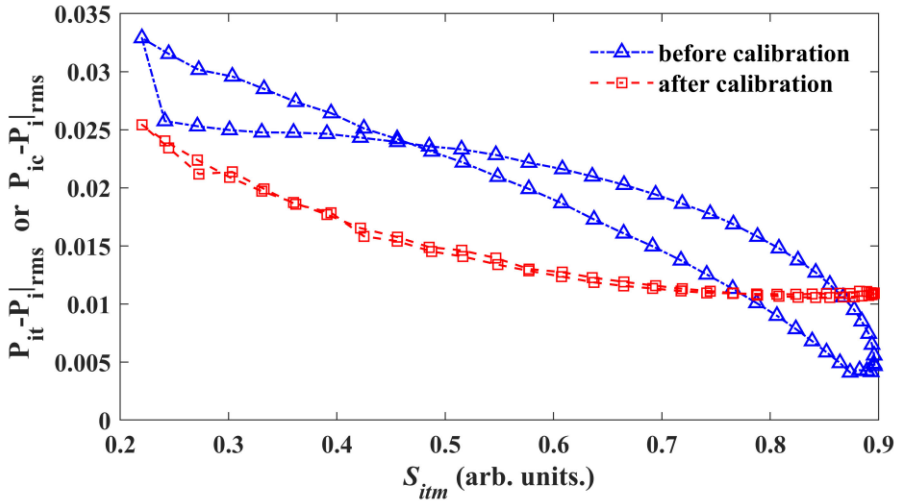

Fig. 6. Measuring errors of DoP before and after calibration under different S_{itm}.

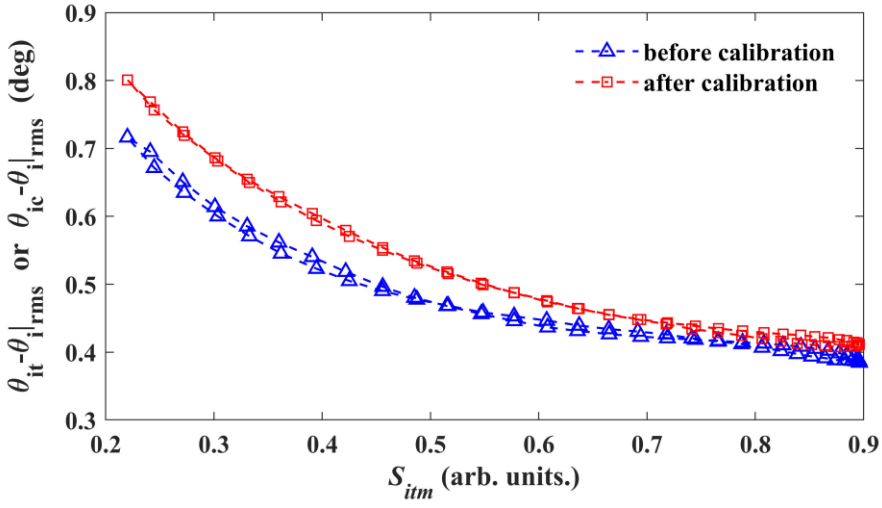

Fig. 7. Measuring errors of AoP before and after calibration under different S_{itm}.

the errors within 3.6% and 0.94 deg respectively for the calibrated DoP and AoP, the proposed calibration method using simple setups can achieve comparable performance [18]–[20].

5. Conclusion

In summary, a calibration method for DoFP polarimeters using nonuniform light has been demonstrated. The principle of this method is explained, and its feasibility is verified by theoretical simulation and experiment. The theoretical simulation shows that there are almost no differences between the input polarization information and the measuring results after calibration, and the experiment results demonstrate that the proposed calibration method can lower the measuring error of polarization information significantly. Compared with other approaches, it can achieve

comparable performance using simple setups, and thus it is expected to be a practical method for the calibration of DoFP polarimeters.

Declaration of Competing Interest: The authors declare that they have no known competing financial interests or personal relationships that could have appeared to influence the work reported in this paper.

References

[1] J. S. Tyo *et al.*, "Review of passive imaging polarimetry for remote sensing applications," *Appl. Opt.*, vol. 45, no. 22, pp. 5453–5469, 2006.

[2] R. Avrahamy *et al.*, "Improving object imaging with sea glinted background using polarization method: Analysis and operator survey," *IEEE Trans. Geosci. Remote Sens.*, vol. 57, no. 11, pp. 8764–8774, Nov. 2019.

[3] Y. Y. Schechner, S. G. Narasimhan, and S. K. Nayar, "Polarization-based vision through haze," *Appl. Opt.*, vol. 42, no. 3, pp. 511–525, 2003.

[4] T. Treibitz and Y. Y. Schechner, "Active polarization descattering," *IEEE Trans. Pattern Anal. Mach. Intell.*, vol. 31, no. 3, pp. 385–399, Mar. 2009.

[5] X. Li *et al.*, "Polarimetric image recovery method combining histogram stretching for underwater imaging," *Sci. Rep.*, vol. 8, pp. 12430, 2018.

[6] M. Garcia *et al.*, "Bio-inspired color-polarization imager for real-time in situ imaging," *Optica*, vol. 4, no. 10, pp. 1263–1271, 2017.

[7] M. Miyata, M. Nakajima, and T. Hashimoto, "Compound-eye metasurface optics enabling a high-sensitivity, ultra-thin polarization camera," *Opt. Exp.*, 28, no. 7, pp. 9996–10014, 2020.

[8] M. Zhang *et al.*, "Polarization-based non-staining cell detection," *Opt. Exp.*, vol. 20, no. 23, pp. 25378–25390, 2012.

[9] T. Novikova *et al.*, "The origins of polarimetric image contrast between healthy and cancerous human colon tissue," *Appl. Phys. Lett.*, vol. 102, no. 24, 2013, Art. no. 241103.

[10] T. Mu *et al.*, "Error analysis of single-snapshot full-Stokes division-of-aperture imaging polarimeters," *Opt. Exp.*, vol. 23, no. 8, pp. 10822–10835, 2015.

[11] O. Morel, R. Seulin, and D. Fofi, "Handy method to calibrate division-of-amplitude polarimeters for the first three stokes parameters," *Opt. Exp.*, vol. 24, no. 12, pp. 13634–13646, 2016.

[12] P. Marconnet *et al.*, "Cancellation of motion artifacts caused by a division-of-time polarimeter," in *Proc. SPIE*, vol. 8160, 2011, Art. no. 81600M.

[13] T. York, R. Marinov, and V. Gruev, "260 frames-per-second 648x488 resolution division-of-focal-plane polarimeter with structural dynamics and tracking applications," *Opt. Exp.*, vol. 24, no. 8, pp. 8243–8252, 2016.

[14] S. Roussel, M. Boffety, and F. Goudail, "On the optimal ways to perform full stokes measurements with a linear division-of-focal-plane polarimetric imager and a retarder," *Opt. Lett.*, vol. 44, no. 11, pp. 2927–2930, 2019.

[15] F. Goudail *et al.*, "Precision of retardance autocalibration in full-Stokes division-of-focal-plane imaging polarimeters," *Opt. Lett.*, vol. 44, no. 22, pp. 5410–5413, 2019.

[16] X. Li *et al.*, "Theory of autocalibration feasibility and precision in full stokes polarization imagers," *Opt. Exp.*, vol. 28, no. 10, pp. 15268–15283, 2020.

[17] F. Zhao *et al.*, "Pixel response model for a division of focal plane polarimeter," *Appl. Opt.*, vol. 58, no. 29, pp. 8109–8117, 2019.

[18] S. B. Powell and V. Gruev, "Calibration methods for division-of-focal-plane polarimeters," *Opt. Exp.*, vol. 21, no. 18, pp. 21039–21055, 2013.

[19] J. Zhang *et al.*, "Non-uniformity correction for division of focal plane polarimeters with a calibration method," *Appl. Opt.*, vol. 55, no. 26, pp. 7236–7240, 2016.

[20] H. Fei *et al.*, "Calibration method for division of focal plane polarimeters," *Appl. Opt.*, vol. 57, no. 18, pp. 4992–4996, 2018.